

1 A Non-homogeneous Time Mixed Integer LP

2 Formulation for Traffic Signal Control

3 Iain Guilliard
4 National ICT Australia
5 7 London Circuit
6 Canberra, ACT, Australia
7 iguilliard@nicta.com.au

8 Scott Sanner
9 Oregon State University
10 1148 Kelley Engineering Center
11 Corvallis, OR 97331
12 scott.sanner@oregonstate.edu

13 Felipe W. Trevizan
14 National ICT Australia
15 7 London Circuit
16 Canberra, ACT, Australia
17 felipe.trevizan@nicta.com.au

18 Brian C. Williams
19 Massachusetts Institute of Technology
20 77 Massachusetts Avenue
21 Cambridge, MA 02139
22 williams@csail.mit.edu

23 4873 words + 8 figures + 0 table + 27 citations
24 (Weighted total words: 6873 out of 7000 + 35 references)
25 August 1, 2015

1 **ABSTRACT**

2 As urban traffic congestion is on the increase worldwide, it is critical to maximize capacity and
3 throughput of existing road infrastructure through optimized traffic signal control. To this end, we
4 build on the body of work in mixed integer linear programming (MILP) approaches that attempt to
5 jointly optimize traffic signal control over an entire traffic network and specifically on improving
6 the scalability of these methods for large numbers of intersections. Our primary insight in this work
7 stems from the fact that MILP-based approaches to traffic control used in a receding horizon con-
8 trol manner (that replan at fixed time intervals) need to compute high fidelity control policies only
9 for the early stages of the signal plan; therefore, coarser time steps can be employed to “see” over
10 a long horizon to preemptively adapt to distant platoons and other predicted long-term changes
11 in traffic flows. To this end, we contribute the queue transmission model (QTM) which blends
12 elements of cell-based and link-based modeling approaches to enable a non-homogeneous time
13 MILP formulation of traffic signal control. We then experiment with this novel QTM-based MILP
14 control in a range of traffic networks and demonstrate that the non-homogeneous MILP formula-
15 tion achieves (i) substantially lower delay solutions, (ii) improved per-vehicle delay distributions,
16 and (iii) more optimal travel times over a longer horizon in comparison to the homogeneous MILP
17 formulation with the same number of binary and continuous variables.

1 INTRODUCTION

2 As urban traffic congestion is on the increase worldwide with estimated productivity losses in the
 3 hundreds of billions of dollars in the U.S. alone and immeasurable environmental impact (1), it is
 4 critical to maximize capacity and throughput of existing road infrastructure through optimized traf-
 5 fic signal control. Unfortunately, many large cities still use some degree of *fixed-time* control (2)
 6 even if they also use *actuated* or *adaptive* control methods such as SCATS (3) or SCOOT (4).
 7 However, there is further opportunity to improve traffic signal control even beyond adaptive meth-
 8 ods through the use of *optimized* controllers (that incorporate elements of both adaptive and actu-
 9 ated control) as evidenced in a variety of approaches including mixed integer (linear) program-
 10 ming (5, 6, 7, 8, 9, 10), heuristic search (11, 12), queuing delay with pressure control (13) and
 11 linear program control (14), to scheduling-driven control (15, 16), and reinforcement learning (2).
 12 Such optimized controllers hold the promise of maximizing existing infrastructure capacity by
 13 finding more complex (and potentially closer to optimal) jointly coordinated intersection policies
 14 in comparison to heuristically-adaptive policies such as SCATS and SCOOT. However, optimized
 15 methods are computationally demanding and often do not guarantee *jointly* optimal solutions over
 16 a large intersection network either because (a) they only consider coordination of neighboring in-
 17 tersections or arterial routes or (b) they fail to scale to large intersection networks simply for com-
 18 putational reasons. We remark that the latter scalability issue is endemic to many mixed integer
 19 programming approaches to optimized signal control.

20 In this work, we build on the body of work in mixed integer linear programming (MILP) ap-
 21 proaches that attempt to jointly optimize traffic signal control over an *entire traffic network* (rather
 22 than focus on arterial routes) and specifically on improving the scalability of these methods for
 23 large urban traffic networks. In our investigation of existing approaches in this vein, namely exem-
 24 plar methods in the spirit of (7, 9) that use a (modified) cell transmission model (CTM) (17, 18) for
 25 their underlying prediction of traffic flows, we remark that a major drawback is the CTM-imposed
 26 requirement to choose a predetermined *homogeneous* (and often necessarily small) time step for
 27 reasonable modeling fidelity. This need to model a large number of CTM cells with a small time
 28 step leads to MILPs that are exceedingly large and often intractable to solve.

29 Our primary insight in this work stems from the fact that MILP-based approaches to traffic
 30 control used in a receding horizon control manner (that replan at fixed time intervals) need to
 31 compute high fidelity control policies only for the early stages of the signal plan; therefore, coarser
 32 time steps can be employed to “see” over a long horizon to preemptively adapt to distant platoons
 33 and other predicted long-term changes in traffic flows. This need for non-homogeneous control in
 34 turn spawns the need for an additional innovation: we require a traffic flow model that permits non-
 35 homogeneous time steps and properly models the travel time delay between lights. To this end,
 36 we might consider CTM extensions such as the variable cell length CTM (19), stochastic CTM
 37 (20, 21), CTM extensions for better modeling freeway-urban interactions (22) including CTM
 38 hybrids with link-based models (23), asymmetric CTMs for better handling flow imbalances in
 39 merging roads (24), the situational CTM for better modeling of boundary conditions (25), and
 40 the lagged CTM for improved modeling of the flow density relation (26). However, despite the
 41 widespread varieties of the CTM and usage for a range of applications (27), there seems to be no
 42 extension that permits *non-homogeneous* time steps as proposed in our novel MILP-based control
 43 approach.

44 For this reason, as a major contribution of this work to enable our non-homogeneous
 45 time MILP-based model of joint intersection control, we contribute the queue transmission model

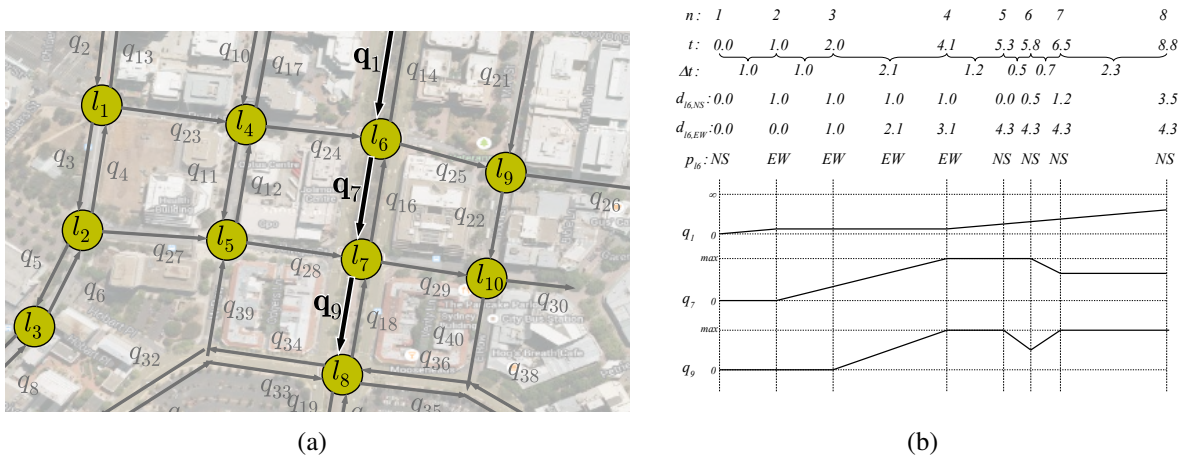


FIGURE 1 (a) Example of a real traffic network modeled using the QTM. (b) A preview of different QTM model parameters as a function of *non-homogeneous* discretized time intervals indexed by n . For each n , we show the following parameters: the elapsed time t , the non-homogeneous time step length Δt , the cumulative duration d of two different light phases for l_6 , the phase p of light l_6 , and the traffic volume of different queues q linearly interpolated between time points. There is technically a binary p for each phase, but we abuse notation and simply show the current active phase: *NS* for *north-south green* and *EW* for *east-west green* assuming the top of the map is north. Here we see that traffic progresses from q_1 to q_7 to q_9 according to light phases and traffic propagation delay with non-homogeneous time steps only at required changepoints. We refer to the QTM model section for precise notation and technical definitions.

(QTM) that blends elements of cell-based and link-based modeling approaches as illustrated and summarized in Figure 1. The QTM offers the following key benefits:

- Unlike previous CTM-based joint intersection signal optimization (7, 9), the QTM is intended for *non-homogeneous* time steps that can be used for control over large horizons.
- Any length of roadway without merges or diverges can be modeled as a single queue leading to compact QTM MILP encodings of large traffic networks (i.e., large numbers of cells and their associated MILP variables are not required *between* intersections). Further, the free flow travel time of a link can be modeled exactly, independent of the discretization time step, while CTM requires a further increased discretization to approach the same resolution.
- The QTM accurately models fixed travel time delays critical to green wave coordination as in (5, 6, 8) through the use of a non-first order Markovian update model and further combines this with fully joint intersection signal optimization in the spirit of (7, 9, 10).

In the remainder of this paper, we first formalize our novel QTM model of traffic flow with non-homogeneous time steps and show how to encode it as a linear program for computing traffic flows. Next we proceed to allow the traffic signals to become discrete phase variables that are optimized subject to a delay minimizing objective and standard minimum and maximum time

constraints for cycles and phases; this results in our final MILP formulation of traffic signal control. We then experiment with this novel QTM-based MILP control in a range of traffic networks and demonstrate that the non-homogeneous MILP formulation achieves (i) substantially lower delay solutions, (ii) improved per-vehicle delay distributions, and (iii) more optimal travel times over a longer horizon in comparison to the homogeneous MILP formulation with the same number of binary and continuous variables.

THE QUEUE TRANSMISSION MODEL (QTM)

A Queue Transmission Model (QTM) is the tuple $(\mathcal{Q}, \mathcal{L}, \vec{\Delta}t, \mathbf{I})$, where \mathcal{Q} and \mathcal{L} are, respectively, the set of queues and lights; $\vec{\Delta}t$ is a vector of size N representing the homogeneous, or non-homogeneous, discretization of the problem horizon $[0, T]$ and the duration in seconds of the n -th time interval is denoted as Δt_n ; and \mathbf{I} is a matrix $|\mathcal{Q}| \times T$ in which $I_{i,n}$ represents the flow of vehicles requesting to enter queue i from the outside of the network at time n .

A **traffic light** $\ell \in \mathcal{L}$ is defined as the tuple $(\Psi_\ell^{\min}, \Psi_\ell^{\max}, \mathcal{P}_\ell, \vec{\Phi}_\ell^{\min}, \vec{\Phi}_\ell^{\max})$, where:

- \mathcal{P}_ℓ is the set of phases of ℓ ;
- Ψ_ℓ^{\min} (Ψ_ℓ^{\max}) is the minimum (maximum) allowed cycle time for ℓ ; and
- $\vec{\Phi}_\ell^{\min}$ ($\vec{\Phi}_\ell^{\max}$) is a vector of size $|\mathcal{P}_\ell|$ and $\Phi_{\ell,k}^{\min}$ ($\Phi_{\ell,k}^{\max}$) is the minimum (maximum) allowed time for phase $k \in \mathcal{P}_\ell$.

A **queue** $i \in \mathcal{Q}$ represents a segment of road that vehicles traverse at free flow speed; once traversed, the vehicles are vertically stacked in a stop line queue. Formally, a queue i is defined by the tuple $(Q_i, T_i^{\text{prop}}, F_i^{\text{out}}, \vec{F}_i, \vec{Pr}_i, \mathcal{Q}_i^{\mathcal{P}})$ where:

- Q_i is the maximum capacity of i ;
- T_i^{prop} is the time required to traverse i and reach the stop line;
- F_i^{out} represents the maximum traffic flow from i to the outside of the modeled network;
- \vec{F}_i and \vec{Pr}_i are vectors of size $|\mathcal{Q}|$ and their j -th entry (i.e., $F_{i,j}$ and $Pr_{i,j}$) represent the maximum flow from queue i to j and the turn probability from i to j (where $\sum_{j \in \mathcal{Q}} Pr_{i,j} = 1$), respectively; and
- $\mathcal{Q}_i^{\mathcal{P}}$ is the set of traffic light phases controlling the outflow of queue i , where the pair, $(\ell, k) \in \mathcal{Q}_i^{\mathcal{P}}$, denotes phase k of light ℓ .

Differently than the CTM (9, 17), the QTM does not assume that $\Delta t_n = T_i^{\text{prop}}$ for all n , that is, the QTM can represent non-homogeneous time intervals (Figure 1(b)). The only requirement over Δt_n is that no traffic light maximum phase time is smaller than any Δt_n since phase changes occur only between time intervals; formally, $\Delta t_n \leq \min_{\ell \in \mathcal{L}, k \in \mathcal{P}_\ell} \Phi_{\ell,k}^{\max}$ for all $n \in \{1, \dots, N\}$.

1 Computing Traffic Flows with QTM

2 In this section, we present how to compute traffic flows using QTM and non-homogeneous time
 3 intervals Δt . We assume for the remainder of this section that a *valid* control plan for all traffic
 4 lights is fixed and given as parameter; formally, for all $\ell \in \mathcal{L}$, $k \in \mathcal{P}_\ell$, and interval $n \in \{1, \dots, N\}$,
 5 the binary variable $p_{\ell,k,n}$ is known a priori and indicates if phase k of light ℓ is active (i.e., $p_{\ell,k,n} =$
 6 1) or not on interval n . Each phase $k \in \mathcal{P}_\ell$ can control the flow from more than one queue, allowing
 7 arbitrary intersection topologies to be modelled, including “all red” phases as a switching penalty
 8 and modeling lost time from amber lights.

9 We represent the problem of finding the maximal flow between capacity-constrained queues
 10 as a Linear Program (LP) over the following variables defined for all intervals $n \in \{1, \dots, N\}$ and
 11 queues i and j :

- 12 • $q_{i,n} \in [0, Q_i]$: traffic volume waiting in the stop line of queue i at the beginning of
 13 interval n ;
- 14 • $f_{i,n}^{\text{in}} \in [0, I_{i,n}]$: inflow to the network via queue i during interval n ;
- 15 • $f_{i,n}^{\text{out}} \in [0, F_i^{\text{out}}]$: outflow from the network via queue i during interval n ; and
- 16 • $f_{i,j,n} \in [0, F_{i,j}]$: flow from queue i into queue j during interval n .

17 The maximum traffic flow from queue i to queue j is enforced by constraints (C1) and (C2).
 18 (C1) ensures that only the fraction $\text{Pr}_{i,j}$ of the total internal outflow of i goes to j , and since each
 19 $f_{i,j,n}$ appears on both sides of (C1), the upstream queue i will block if any downstream queue j
 20 is full. (C2) forces the flow from i to j to be zero if all phases controlling i are inactive (i.e.,
 21 $p_{\ell,k,n} = 0$ for all $(\ell, k) \in \mathcal{Q}_i^{\mathcal{P}}$). If more than one phase $p_{\ell,k,n}$ is active, then (C2) is subsumed by
 22 the domain upper bound of $f_{i,j,n}$.

$$23 \quad f_{i,j,n} \leq \text{Pr}_{i,j} \sum_{k=1}^{|\mathcal{Q}|} f_{i,k,n} \quad (\text{C1})$$

$$24 \quad f_{i,j,n} \leq F_{i,j} \sum_{(l,k) \in \mathcal{Q}_i^{\mathcal{P}}} p_{l,k,n} \quad (\text{C2})$$

26 To simplify the presentation of the remainder of the LP, we define the helper variables
 27 $q_{i,n}^{\text{in}}$ (C3), $q_{i,n}^{\text{out}}$ (C4), and t_n (C5) to represent the volume of traffic to enter and leave queue i during
 28 interval n , and the time elapsed since the beginning of the problem until the end of interval Δt_n ,
 29 respectively.

$$30 \quad q_{i,n}^{\text{in}} = \Delta t_n (f_{i,n}^{\text{in}} + \sum_{j=1}^{|\mathcal{Q}|} f_{j,i,n}) \quad (\text{C3})$$

$$31 \quad q_{i,n}^{\text{out}} = \Delta t_n (f_{i,n}^{\text{out}} + \sum_{j=1}^{|\mathcal{Q}|} f_{i,j,n}) \quad (\text{C4})$$

$$32 \quad t_n = \sum_{x=1}^n \Delta t_x \quad (\text{C5})$$

33

In order to account for the misalignment of the different Δt and T_i^{prop} , we need to find the volume of traffic that entered queue i between two arbitrary points in time x and y ($x \in [0, T]$, $y \in [0, T]$, and $x < y$), i.e., x and y might not coincide with any t_n for $n \in \{1, \dots, N\}$. This volume of traffic, denoted as $V_i(x, y)$, is obtained by integrating $q_{i,n}^{\text{in}}$ over $[x, y]$ and is defined in (1) where m and w are the index of the time intervals s.t. $t_m \leq x < t_{m+1}$ and $t_w \leq y < t_{w+1}$. Because the QTM dynamics are *piecewise linear*, $q_{i,n}^{\text{in}}$ is a step function w.r.t. time and this integral reduces to the sum of $q_{i,n}^{\text{in}}$ over the intervals contained in $[x, y]$ and the appropriate fraction of $q_{i,m}^{\text{in}}$ and $q_{i,w}^{\text{in}}$ representing the misaligned beginning and end of $[x, y]$.

$$V_i(x, y) = (t_{m+1} - x) \frac{q_{i,m}^{\text{in}}}{\Delta t_m} + \left(\sum_{k=m+1}^{w-1} q_{i,k}^{\text{in}} \right) + (y - t_w) \frac{q_{i,w}^{\text{in}}}{\Delta t_w} \quad (1)$$

Using these helper variables, (C6) represents the flow conservation principle for queue i where $V_i(t_{n-1} - T_i^{\text{prop}}, t_n - T_i^{\text{prop}})$ is the volume of vehicles that reached the stop line during Δt_n . Since Δt and T_i^{prop} for all queues are known a priori, the indexes m and w used by V_i can be pre-computed in order to encode (1); moreover, (C6) represents a non-first order Markovian update because the update considers the previous $w - m$ time steps. To ensure that the total volume of traffic traversing i (i.e., $V_i(t_n - T_i^{\text{prop}}, t_n)$) and waiting at the stop line does not exceed the capacity of the queue, we apply (C7). When queue i is full, $q_{i,n}^{\text{in}} = 0$ by (C7), which forces $f_{j,i,n}$ to 0 in (C3) and (C4). This in turn allows the queue in i to spill back into the upstream queue j .

$$q_{i,n} = q_{i,n-1} - q_{i,n-1}^{\text{out}} + V_i(t_{n-1} - T_i^{\text{prop}}, t_n - T_i^{\text{prop}}) \quad (\text{C6})$$

$$V_i(t_n - T_i^{\text{prop}}, t_n) + q_{i,n} \leq Q_i \quad (\text{C7})$$

As with MILP formulations of CTM (e.g. Lin and Wang (9)), QTM is also susceptible to *withholding traffic*, i.e., the optimizer might prevent vehicles from moving from i to j even though the associated traffic phase is active and j is not full, e.g., this may reserve space for traffic from an alternate approach that allows the MILP to minimize delay in the long-term even though it leads to unintuitive traffic flow behavior. We address this well-known issue through our objective function (O1) by maximizing the total outflow $q_{i,n}^{\text{out}}$ (i.e., both internal and external outflow) of i plus the inflow $f_{i,n}^{\text{in}}$ from the outside of the network to i . This quantity is weighted by the remaining time until the end of the problem horizon T to force the optimizer to allow as much traffic volume as possible into the network and move traffic to the outside of the network as soon as possible.

$$\max \sum_{n=1}^N \sum_{i=1}^{|Q|} (T - t_n + 1) (f_{i,n}^{\text{out}} + f_{i,n}^{\text{in}}) \quad (\text{O1})$$

The objective (O1) corresponds to minimizing delay in CTM models, e.g., (O1) is equivalent to the objective function (O3) in Lin and Wang (9) for their parameters $\alpha = 1$, $\beta = 1$ for the origin cells, and $\beta = 0$ for all other cells. Figure 2 depicts this equivalence using the cumulative number of vehicles entering and leaving a network as a function of time. The delay experienced by the vehicles travelling through this network (red curve in Figure 2) equals the horizontal difference at each point between the cumulative departure and arrival curves (less the free flow travel time through the network). Maximizing $f_{i,n}^{\text{out}}$ weighted by $(T - t_n + 1)$ in (O1) is the same as forcing the departure curve to be as close as possible to the arrival curve as early as possible; therefore, the area between arrival and departure is minimized, which in turn minimizes the delay.

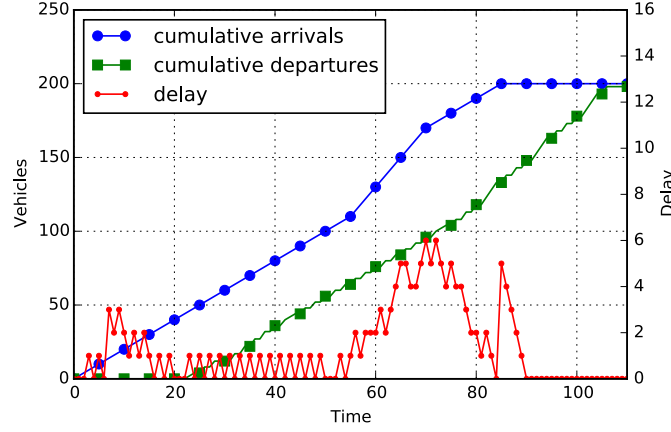


FIGURE 2 Cumulative arrival (blue) and departure (green) curves, and the delay curve (red) resulting from the horizontal difference between the arrival and departure curves, less the free flow travel time. The arrival curve is fixed by the demand profile, and the departure curve is maximized by the objective function (O1), which has the same effect as minimizing the area under the delay curve.

To illustrate the representation tradeoff offered by non-homogeneous time intervals, we computed flows and queue volumes for a fixed signal control plan derived for homogeneous $\Delta t_n = 1\text{s}$ (ground truth) using different discretizations. Figure 3(a) shows the approximation of the ground truth using homogeneous $\Delta t = 2.5$ and $\Delta t = 5.0$, and Figure 3(b) using non-homogeneous time intervals that linearly increases from 1s to 2.5s, i.e., $\Delta t_n \approx 0.0956n + 0.9044$ for $n \in \{1, \dots, 17\}$. As Figure 3(a) shows, large time steps can be rough approximations of the ground truth. Non-homogeneous discretization (Figure 3(b)) exploit this fact to provide a good approximation in the initial time steps and progressively decrease precision for points far in the future.

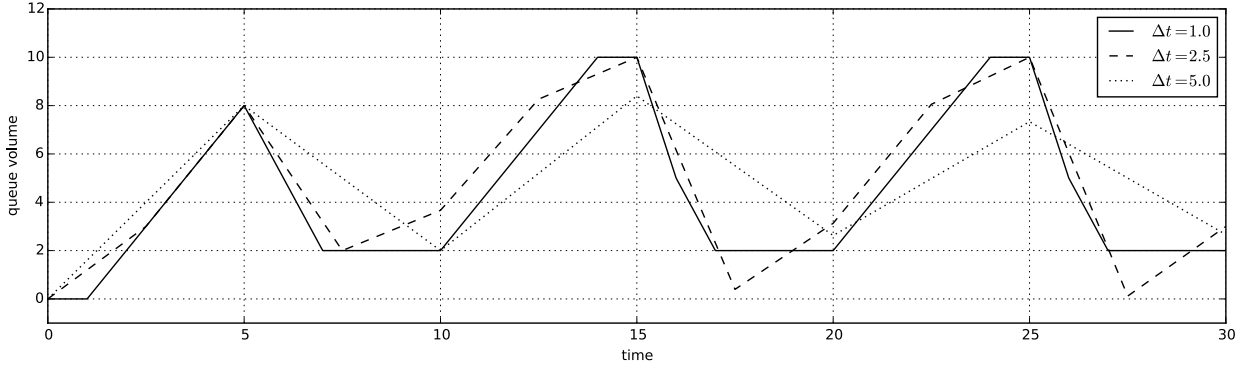
TRAFFIC CONTROL WITH QTM ENCODED AS A MILP

In this section, we remove the assumption that a valid control plan for all traffic lights is given and extend the LP (O1, C1–C7) to an Mixed-Integer LP (MILP) that also computes the optimal control plan. Formally, for all $\ell \in \mathcal{L}$, $k \in \mathcal{P}_\ell$, and interval $n \in \{1, \dots, N\}$, the phase activation parameter $p_{\ell,k,n} \in \{0, 1\}$ becomes a free variable to be optimized. In order to obtain a valid control plan, we enforce that one phase of traffic light ℓ is always active at any interval n (C8), and ensure cyclic phase polices where phase changes follow a fixed ordered sequence (C9), i.e., if phase k was active during interval $n - 1$ and has become inactive in interval n , then phase $k + 1$ must be active in interval n . (C9) assumes that $k + 1$ equals 1 if $k = |\mathcal{P}_\ell|$.

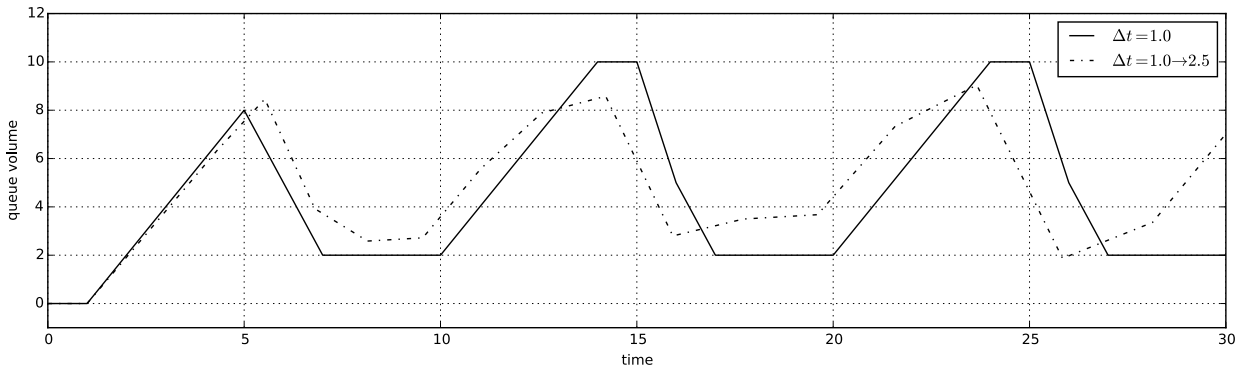
$$\sum_{k=1}^{|\mathcal{P}_\ell|} p_{\ell,k,n} = 1 \quad (\text{C8})$$

$$p_{\ell,k,n-1} \leq p_{\ell,k,n} + p_{\ell,k+1,n} \quad (\text{C9})$$

Next, we enforce the minimum and maximum phase durations (i.e., $\Phi_{\ell,k}^{\min}$ and $\Phi_{\ell,k}^{\max}$) for each phase $k \in \mathcal{P}_\ell$ of traffic light ℓ . To encode these constraints, we use the helper variable



(a)



(b)

FIGURE 3 Approximations of a queue volume obtained using homogeneous $\vec{\Delta t} = \{1.0, \dots, 1.0\}$ using: (a) homogeneous $\vec{\Delta t} = \{2.5, \dots, 2.5\}$ and $\vec{\Delta t} = \{5.0, \dots, 5.0\}$; and (b) non-homogeneous $\vec{\Delta t} = \{1.0, 1.05, 1.1, 1.16, \dots, 2.29, 2.41, 2.5\}$ where $\Delta t_n \approx 0.0956n + 0.9044$ for $n \in \{1, \dots, 17\}$. Here we see that (b) achieves accuracy in the near-term that somewhat degrades over the long-term, where accuracy will be less critical for receding horizon control.

1 $d_{\ell,k,n} \in [0, \Phi_{\ell,k}^{\max}]$, defined by constraints (C10–C14), that: (i) holds the elapsed time since the
2 start of phase k when $p_{\ell,k,n}$ is active (C10,C11); (ii) is constant and holds the duration of the last
3 phase until the next activation when $p_{\ell,k,n}$ is inactive (C12,C13); and (iii) is restarted when phase k
4 changes from inactive to active (C14). Notice that (C10–C14) employs the *big-M* method to turn
5 the cases that should not be active into subsumed constraints based on the value of $p_{\ell,k,n}$. We
6 use $\Phi_{\ell,k}^{\max}$ as our large constant since $d_{\ell,k,n} \leq \Phi_{\ell,k}^{\max}$ and $\Delta t_n \leq \Phi_{\ell,k}^{\max}$. Similarly, constraint (C15)
7 ensures the minimum phase time of k and is not enforced while k is still active. Figures 4(a)
8 to 4(c) present an example of how (C10–C15) work together as a function of the time n for $d_{\ell,k,n}$;

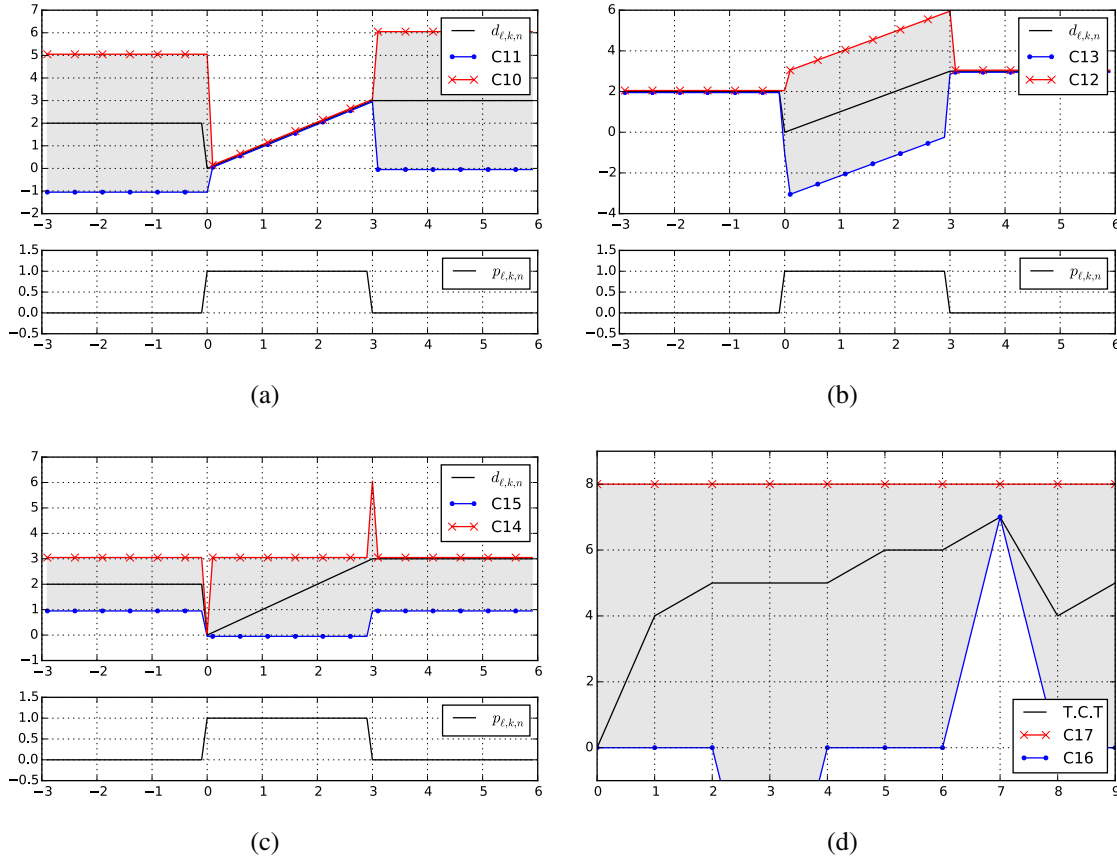


FIGURE 4 Visualization of constraints (C10–C17) for a traffic light ℓ as a function of time. (a–c) present, pairwise, the constraints (C10–C15) for phase k ($d_{\ell,k,n}$ as the black line) and the activation variable $p_{\ell,k,n}$ in the small plot. (d) presents the constraints for the cycle time of ℓ (C16 and C17), where T.C.T. is the total cycle time and is the left hand side of both constraints. For this example, $\Phi_{\ell,k}^{\min} = 1$, $\Phi_{\ell,k}^{\max} = 3$, $\Psi_{\ell}^{\min} = 7$, and $\Psi_{\ell}^{\max} = 8$.

1 the domain constraint $0 \leq d_{\ell,k,n} \leq \Phi_{\ell,k}^{\max}$ for all $n \in \{1, \dots, N\}$ is omitted for clarity.

$$2 \quad d_{\ell,k,n} \leq d_{\ell,k,n-1} + \Delta t_{n-1} p_{\ell,k,n-1} + \Phi_{\ell,k}^{\max} (1 - p_{\ell,k,n-1}) \quad (\text{C10})$$

$$3 \quad d_{\ell,k,n} \geq d_{\ell,k,n-1} + \Delta t_{n-1} p_{\ell,k,n-1} - \Phi_{\ell,k}^{\max} (1 - p_{\ell,k,n-1}) \quad (\text{C11})$$

$$4 \quad d_{\ell,k,n} \leq d_{\ell,k,n-1} + \Phi_{\ell,k}^{\max} p_{\ell,k,n-1} \quad (\text{C12})$$

$$5 \quad d_{\ell,k,n} \geq d_{\ell,k,n-1} - \Phi_{\ell,k}^{\max} p_{\ell,k,n} \quad (\text{C13})$$

$$6 \quad d_{\ell,k,n} \leq \Phi_{\ell,k}^{\max} (1 - p_{\ell,k,n} + p_{\ell,k,n-1}) \quad (\text{C14})$$

$$7 \quad d_{\ell,k,n} \geq \Phi_{\ell,k}^{\min} (1 - p_{\ell,k,n}) \quad (\text{C15})$$

9 Lastly, we constrain the sum of all the phase durations for light ℓ to be within the cycle
 10 time limits Ψ_{ℓ}^{\min} (C16) and Ψ_{ℓ}^{\max} (C17). In both (C16) and (C17), we use the duration of phase 1
 11 of ℓ from the previous interval $n - 1$ instead of the current interval n because (C14) forces $d_{\ell,1,n}$ to
 12 be 0 at the beginning of each cycle; however, from the previous end of phase 1 until $n - 1$, $d_{\ell,1,n-1}$
 13 holds the correct elapse time of phase 1. Additionally, (C16) is enforced right after the end of the

1 each cycle, i.e., when its first phase is changed from inactive to active. The value (C16) and (C17)
 2 over time for a traffic light ℓ is illustrated in Figure 4(d).

$$3 \quad d_{\ell,1,n-1} + \sum_{k=2}^{|\mathcal{P}_\ell|} d_{\ell,k,n} \geq \Psi_\ell^{\min}(p_{\ell,1,n} - p_{\ell,1,n-1}) \quad (\text{C16})$$

$$4 \quad d_{\ell,1,n-1} + \sum_{k=2}^{|\mathcal{P}_\ell|} d_{\ell,k,n} \leq \Psi_\ell^{\max} \quad (\text{C17})$$

6 The MILP that encodes the problem of finding the optimal traffic control plan in a QTM network
 7 is defined by (O1, C1–C17).

8 **EMPIRICAL EVALUATION**

9 In this section we compare the solutions for traffic networks modeled as a QTM using homo-
 10 geneous and non-homogeneous time intervals w.r.t. to two evaluation criteria: the quality of the
 11 solution and convergence to the optimal solution vs. the number of time steps. Specifically, we
 12 compare the quality of solutions based on the total travel time and we also consider the third quar-
 13 tile and maximum of the observed delay distribution. The hypotheses we wish to evaluate in this
 14 paper are: (i) the quality of the non-homogeneous solutions is at least as good as the homoge-
 15 neous ones when the number of time intervals N is fixed; and (ii) the non-homogeneous approach
 16 requires less time intervals (i.e., smaller N) than the homogeneous approach to converge to the
 17 optimal solution. In the remainder of this section, we present the traffic networks considered in the
 18 experiments, our methodology, and the results.

19 **Networks**

20 We consider three networks of increasing complexity (Figure 5): an avenue crossed by three side
 21 streets; a 2-by-3 grid; and a 3-by-3 grid with a diagonal avenue. The queues receiving vehicles
 22 from outside of the network are marked in Figure 5 and we refer to them as input queues. The
 23 maximum queue capacity (Q_i) is 60 vehicles for non-input queues and infinity for input queues to
 24 prevent interruption of the input demand due to spill back from the stop line. The traversal time of
 25 each queue i (T_i^{prop}) is set at 9s (a distance of 125m with a free flow speed of 50km/h). For each
 26 street, flows are defined from the head of each queue i into the tail of the next queue j ; there is no
 27 turning traffic ($\text{Pr}_{i,j} = 1$), and the maximum flow rate between queues, $F_{i,j}$, is set at 5 vehicles/s.
 28 All traffic lights have two phases, north-south and east-west, and lights 2, 4 and 6 of network 3
 29 have the additional northeast-southwest phase to control the diagonal avenue. For networks 1 and
 30 2, $\Phi_{\ell,k}^{\min}$ is 1s, $\Phi_{\ell,k}^{\max}$ is 3s, Ψ_ℓ^{\min} is 2s, and Ψ_ℓ^{\max} is 6s, for all traffic light ℓ and phase k . For network
 31 3, $\Phi_{\ell,k}^{\min}$ is 1s and $\Phi_{\ell,k}^{\max}$ is 6s for all ℓ and k ; and Ψ_ℓ^{\min} is 2s and Ψ_ℓ^{\max} is 12s for all lights ℓ except
 32 for lights 2, 4 and 6 (i.e., lights also used by the diagonal avenue) in which Ψ_ℓ^{\min} is 3s and Ψ_ℓ^{\max} is
 33 18s.

34 **Experimental Methodology**

35 For each network, a constant background level traffic is injected in the network in the first 55s to
 36 allow the solver to settle on a stable policy. Then a spike in demand is introduced in the queues
 37 marked as ♠ (Figure 5) from time 55s to 70s to trigger a policy change. From time 70s to 85s,
 38 the demand is returned to the background level, and then reduced to zero for all input queues. We

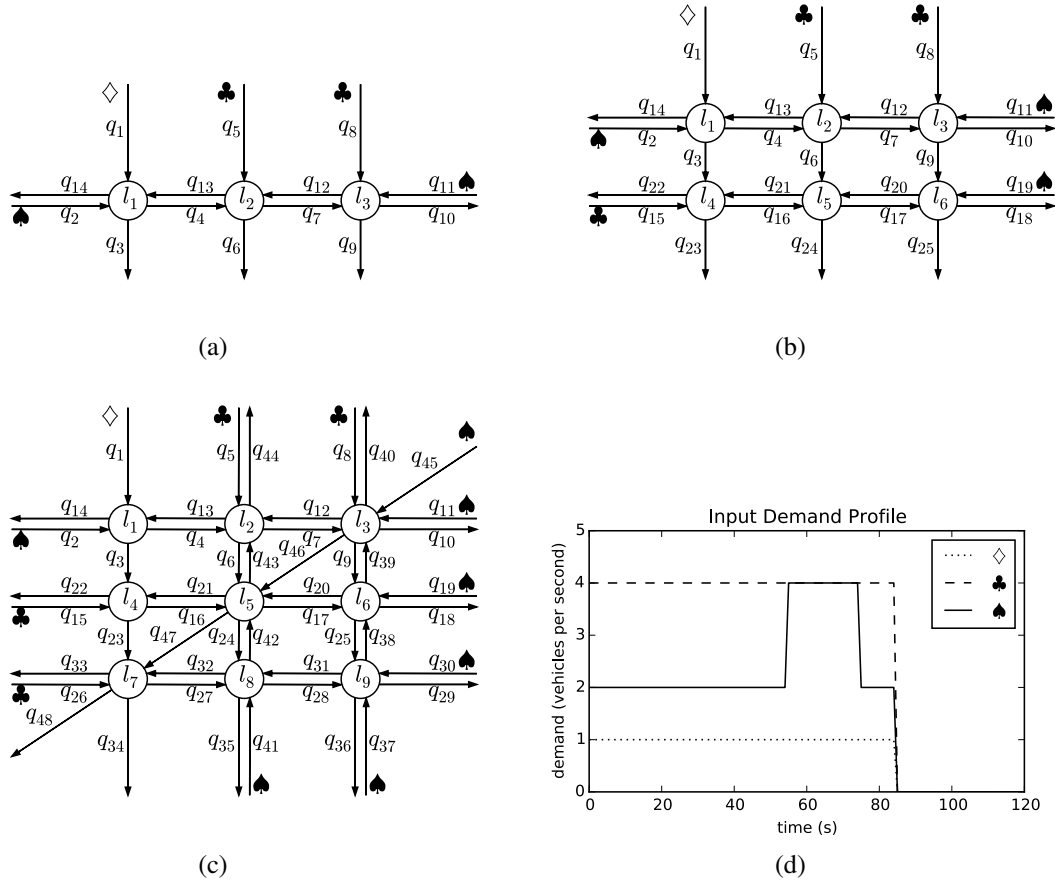


FIGURE 5 (a–c) Networks used to evaluate the QTM performance. (d) Demand profile of the queues marked as \diamond , \clubsuit , and \spadesuit for our experiments.

1 extend the problem horizon T until all vehicles have left the network. By clearing the network,
 2 we can easily measure the total travel time for all the traffic as the area between the cumulative
 3 arrival and departure curves measured at the boundaries of the network. The background level
 4 for the input queues are 1, 4 and 2 vehicles/s for queues marked as \diamond , \clubsuit and \spadesuit (Figure 5(d)),
 5 respectively; and during the high demand period, the queues \spadesuit receive 4 vehicles/s.

6 For both homogeneous and non-homogeneous intervals, we use the MILP QTM formula-
 7 tion in a receding horizon manner: a control plan is computed for a pre-defined horizon (smaller
 8 than T) and only a prefix of this plan is executed before generating a new control plan. Figure 6(a)
 9 depicts our receding horizon approach and we refer to the planning horizon as a major frame and
 10 its executable prefix as a minor frame. Notice that, while the plan for a minor frame is being
 11 executed, we can start computing the solution for the next major frame based on a forecast model.

12 To perform a fair comparison between the homogeneous and non-homogeneous discretiza-
 13 tions, we fix the size of all minor frames to 10s and force it to be discretized in homogeneous
 14 intervals of 0.25s. For the homogeneous experiments, Δt is kept at 0.25s throughout the major
 15 frame; therefore, given N , the major frame size equals $N/4$ seconds for the homogeneous ap-
 16 proach. For the non-homogeneous experiments, we increase Δt linearly from the end of the minor
 17 frame for 10s and then hold it constant to the end of the major frame. We use two discretizations as

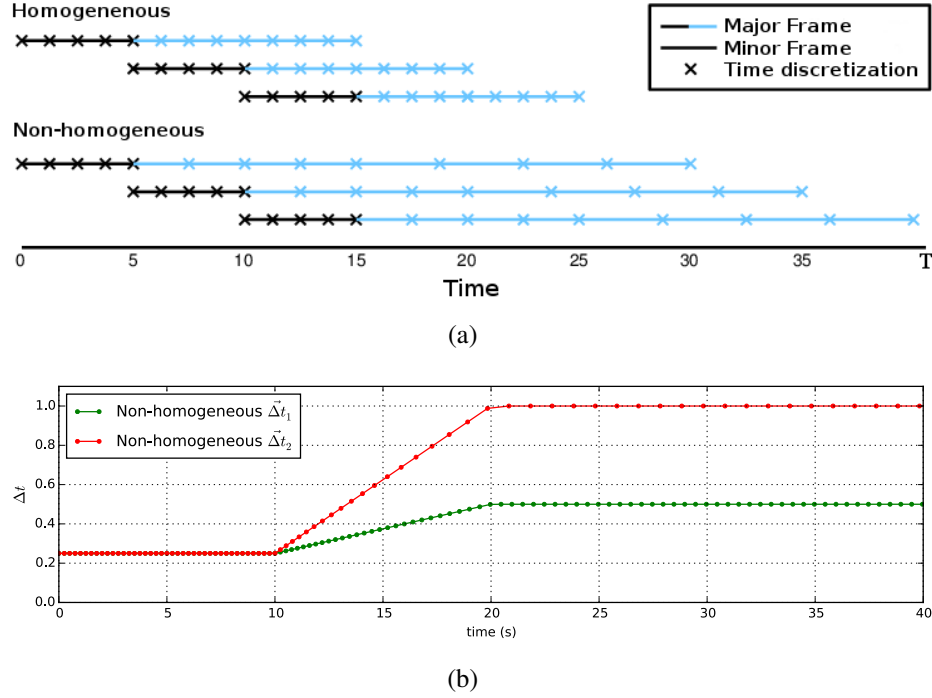


FIGURE 6 (a) Receding horizon control. In this example, the problem horizon T is 40s. The major frames for MILP optimization are discretized in 12 time intervals ($N = 12$) and they span 15s and 30s for homogeneous and non-homogeneous discretizations, respectively. The minor frames represent the prefix of the major frame MILP optimization that is executed. The horizon recedes by the minor frame duration after each execution. (b) The two non-homogeneous discretizations used in the experiments, shown here with a major frame duration of 40s. From the end of the minor frame time, Δt is linearly interpolated over 10s, from 0.25 to 0.5 for Non-homogeneous $\vec{\Delta t}_1$, and 0.25 to 1.0 for Non-homogeneous $\vec{\Delta t}_2$. Δt is then held constant to the end of the major frame time.

1 shown in Figure 6(b): Non-homogeneous $\vec{\Delta t}_1$ from 0.25 to 0.5, and Non-homogeneous $\vec{\Delta t}_2$ from
 2 0.25 to 1.0. For a given $N > 40$, the major frame size used by this non-homogeneous approach
 3 is $10.375 + 1.25(N - 40)$ seconds for $\vec{\Delta t}_1$, and $10.375 + 0.625(N - 40)$ seconds for $\vec{\Delta t}_2$. Once
 4 we have generated a series of minor frames, we concatenate them into a single plan and compute
 5 the flow through the network using the QTM LP formulation with a fixed (homogeneous) Δt of
 6 0.25s. We also compare both receding horizon approaches against the optimal solution obtained
 7 by computing a single control plan for the entire control horizon (i.e., $[0, T]$) using a fixed Δt of
 8 0.25s.

9 For all our experiments, we used GurobiTM as the MILP solver with 12 threads on a 3.1GHz
 10 AMD OpteronTM 4334 processor with 12 cores. We limit the MIP gap accuracy to 0.1% and the
 11 time cutoff for solving a major frame to 3000s for the receding horizon approaches and unbounded
 12 in order to determine the optimal minimum travel run time solution to which all other solutions are
 13 compared. All our results are averaged over five runs to account for Gurobi's stochastic strategies.

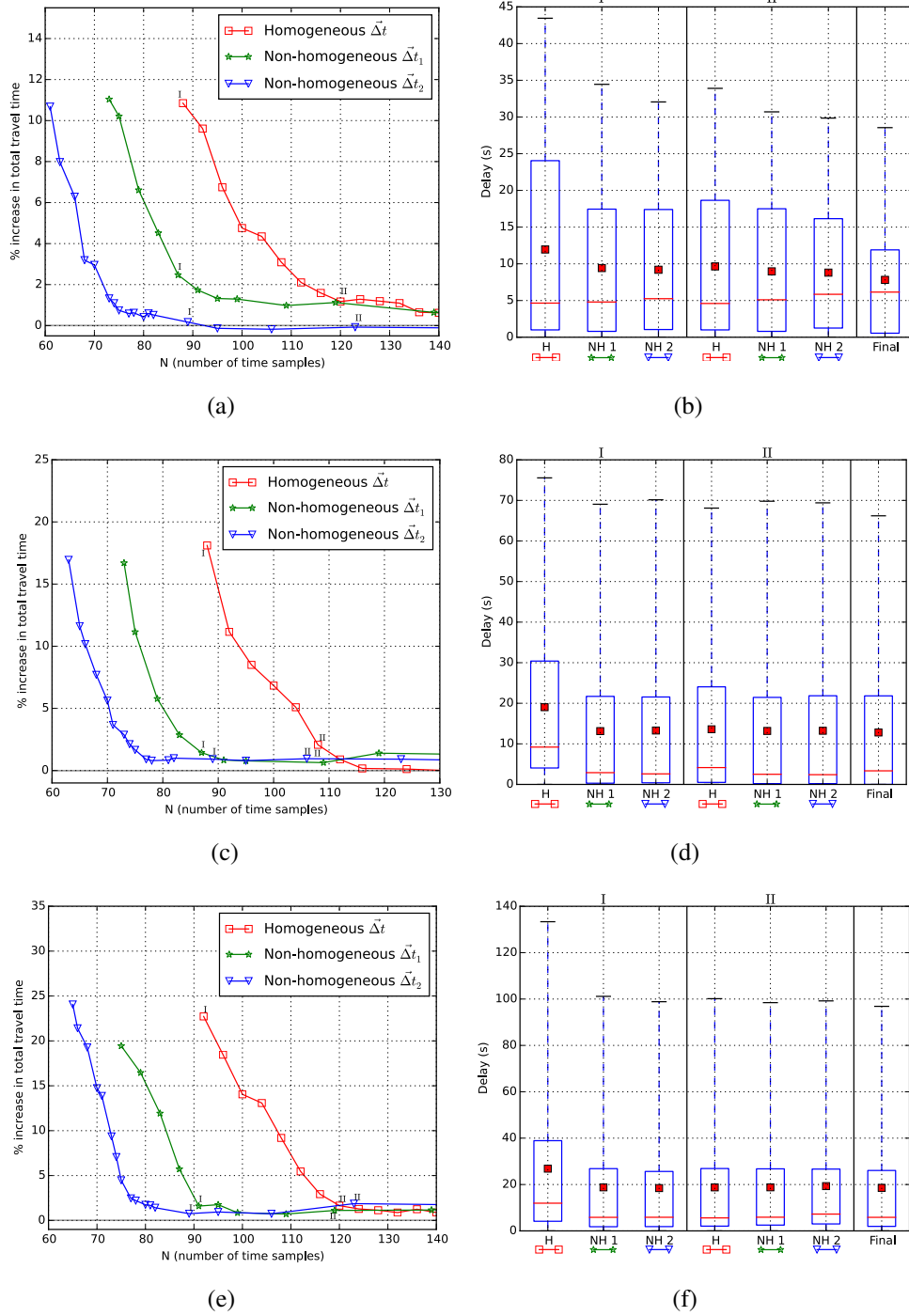


FIGURE 7 Increase in the total travel time w.r.t. the optimal solution as a function of N (a,c,e) and distribution of the total delay of each car for different values of N (b,d,f). For each row, the Roman numeral on top of the box plots corresponds to points on the travel time plot marked with the same numeral. The mean of the total delay is presented as a red square in the box plots. Plots in the i -th row correspond to the results for the i -th network in Figure 5. Non-homogeneous (NH) achieves much better solutions at smaller N than Homogeneous (H).

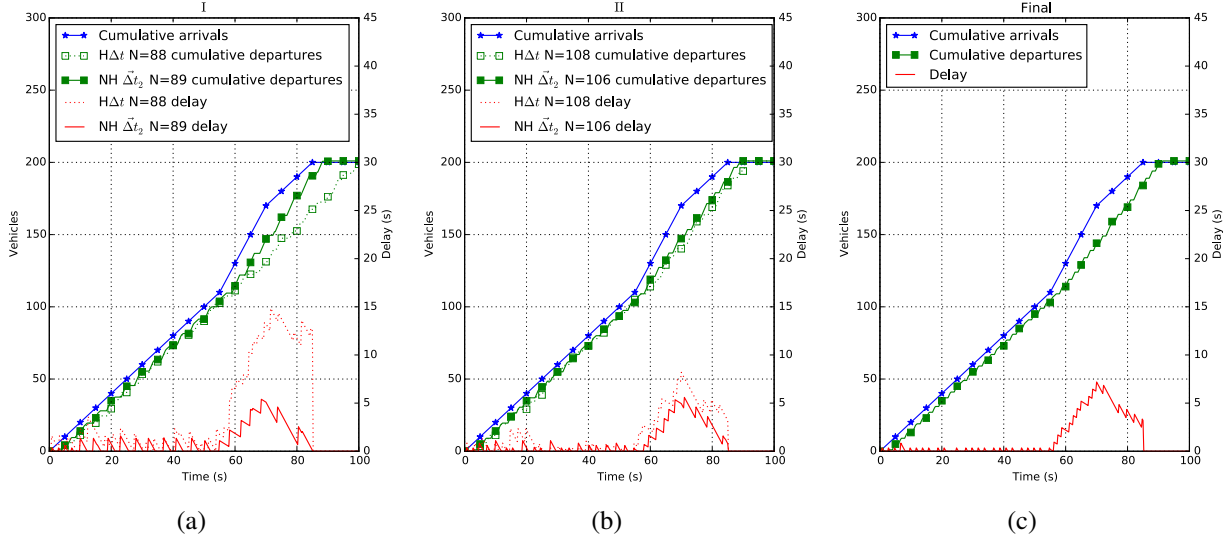


FIGURE 8 Cumulative arrival and departure curves and delay for queue 1 in the 2-by-3 network (Figure 5(b)). The labels on top of each plot match the labels in Figures 7(c) and 7(d). (c) presents the same curves for the optimal solution. Non-homogeneous ($\vec{\Delta}t_2$) provides near-optimal signal plans over a longer time horizon than Homogeneous (H) when the number of time intervals N is small.

1 Results

2 Figures 7(a), 7(c) and 7(e) show, for each network, the increase in the total travel time w.r.t. the
 3 optimal solution as a function of N . As we hypothesized, the non-homogeneous discretizations
 4 requires less time intervals (i.e., smaller N) to obtain a solution with the same total travel time,
 5 and $\vec{\Delta}t_2$ converges before $\vec{\Delta}t_1$. This is important because the size of the MILP, including the
 6 number of binary variables, scales linearly with N ; therefore, the non-homogeneous approach can
 7 scale up better than the homogeneous one (e.g., Figure 7(e)). Also, for homogeneous and non-
 8 homogeneous discretizations, finding the optimal solution of major frames with large N might
 9 require more time than our imposed 3000s time cutoff and, in this case, Gurobi returns a feasible
 10 control plan that is far from optimal. The effect in the total travel time of these poor solutions can
 11 be seen in Figure 7(e) for $N > 120$.

12 The distribution of the total delay observed by each vehicle while traversing the network
 13 is shown in Figures 7(b), 7(d) and 7(f). Each group of box plots represents a different value of N :
 14 when the non-homogeneous $\vec{\Delta}t_2$ first converges; when the homogeneous Δt first converges; and
 15 the final solution itself. In all networks, the quality of the solutions obtained using both of the $\vec{\Delta}t_1$
 16 and $\vec{\Delta}t_2$ and is better or equal than using homogeneous Δt for fixed N in both the total travel time
 17 and *fairness*, i.e., smaller third quartile and maximum delay.

18 To further illustrate the differences between homogeneous and non-homogeneous discretiza-
 19 tions, Figure 8 shows the cumulative arrival and departure curves and the how delay evolves
 20 over time for q_1 of network 2 (Figure 5(b)). In Figure 8(a), the comparison is done when non-
 21 homogeneous $\vec{\Delta}t_2$ first converges (i.e., point I in Figure 7(c)) and for this value of N , the major
 22 frame size in seconds of the non-homogeneous approach is 19.125s longer than the homogeneous
 23 one. This allows the MILP solver to “see” 19s further in the future when using non-homogeneous

discretization and find a coordinated signal policy along the avenue to dissipate the extra traffic that arrives at time 55s. The shorter major frame of the homogeneous discretization does not allow the solver to adapt this far in advance and its delay observed after 55s is much larger than the non-homogeneous one. Once the homogeneous Δt has converged (Figure 8(b)), it is also able to anticipate the increased demand and adapt well in advance and both approaches generate solutions close to optimum (Figure 8(c)).

CONCLUSION

In this paper, we showed how to formulate a novel queue transmission model (QTM) of traffic flow with non-homogeneous time steps as a linear program. We then proceeded to allow the traffic signals to become discrete variables subject to a delay minimizing optimization objective and standard traffic signal constraints leading to a final MILP formulation of traffic signal control with non-homogeneous time steps. We experimented with this novel QTM-based MILP control in a range of traffic networks and demonstrated that the non-homogeneous MILP formulation achieved (i) substantially lower delay solutions, (ii) improved per-vehicle delay distributions, and (iii) more optimal travel times over a longer horizon in comparison to the homogeneous MILP formulation with the same number of binary and continuous variables. Altogether, this work represents a major step forward in the scalability of MILP-based jointly optimized traffic signal control via the use of a non-homogeneous time traffic models and thus helps pave the way for fully optimized joint urban traffic signal controllers as an improved successor technology to existing signal control methods.

Our future work includes learning the QTM parameters (e.g., turn probabilities $Pr_{i,j}$ and expected incoming flows $I_{i,n}$) from loop detector data, and evaluating the impact in scalability of different non-homogeneous discretizations and size of the computer cluster used for computing the control plans.

ACKNOWLEDGMENT

This work is part of the Advanced Data Analytics in Transport programme, and supported by National ICT Australia (NICTA) and NSW Trade & Investment. NICTA is funded by the Australian Government through the Department of Communications and the Australian Research Council through the ICT Centre of Excellence Program. NICTA's role is to pursue potentially economically significant ICT related research for the Australian economy. NSW Trade & Investment is the business development agency for the State of New South Wales.

REFERENCES

- [1] Bazzan, A. L. C. and F. Klügl, *Introduction to Intelligent Systems in Traffic and Transportation*. Synthesis Lectures on Artificial Intelligence and Machine Learning, Morgan & Claypool Publishers, 2013.
- [2] El-Tantawy, S., B. Abdulhai, and H. Abdelgawad, Multiagent reinforcement learning for integrated network of adaptive traffic signal controllers (MARLIN-ATSC): methodology and large-scale application on downtown Toronto. *Intelligent Transportation Systems, IEEE Transactions on*, Vol. 14, No. 3, 2013, pp. 1140–1150.
- [3] Sims, A. G. and K. W. Dobinson, SCAT—The Sydney co-ordinated adaptive traffic system: Philosophy and benefits. *IEEE Transactions on Vehicular Technology*, Vol. 29, 1980.

- [4] Hunt, P. B., D. I. Robertson, R. D. Bretherton, and R. I. Winton, *SCOOT—A traffic responsive method of coordinating signals*. Transportation Road Research Lab, Crowthorne, U.K., 1981.
- [5] Gartner, N., J. D. Little, and H. Gabbay, *Optimization of traffic signal settings in networks by mixed-integer linear programming*. DTIC Document, 1974.
- [6] Gartner, N. H. and C. Stamatiadis, Arterial-based control of traffic flow in urban grid networks. *Mathematical and computer modelling*, Vol. 35, No. 5, 2002, pp. 657–671.
- [7] Lo, H. K., A novel traffic signal control formulation. *Transportation Research Part A: Policy and Practice*, Vol. 33, No. 6, 1998, pp. 433–448.
- [8] He, Q., K. L. Head, and J. Ding, PAMSCOD: Platoon-based Arterial Multi-modal Signal Control with Online Data. *Procedia-Social and Behavioral Sciences*, Vol. 17, 2011, pp. 462–489.
- [9] Lin, W.-H. and C. Wang, An enhanced 0-1 mixed-integer LP formulation for traffic signal control. *Intelligent Transportation Systems, IEEE Transactions on*, Vol. 5, No. 4, 2004, pp. 238–245.
- [10] Han, K., T. L. Friesz, and T. Yao, A link-based mixed integer LP approach for adaptive traffic signal control. *arXiv preprint arXiv:1211.4625*, 2012.
- [11] Lo, H. K., E. Chang, and Y. C. Chan, Dynamic network traffic control. *Transportation Research Part A: Policy and Practice*, Vol. 35, No. 8, 1999, pp. 721–744.
- [12] He, Q., W.-H. Lin, H. Liu, and K. L. Head, Heuristic algorithms to solve 0–1 mixed integer LP formulations for traffic signal control problems. In *Service Operations and Logistics and Informatics (SOLI), 2010 IEEE International Conference on*, IEEE, 2010, pp. 118–124.
- [13] Varaiya, P., Max pressure control of a network of signalized intersections. *Transportation Research Part C: Emerging Technologies*, Vol. 36, 2013, pp. 177–195.
- [14] Li, J. and H. Zhang, Coupled Linear Programming Approach for Decentralized Control of Urban Traffic. *Transportation Research Record: Journal of the Transportation Research Board*, No. 2439, 2014, pp. 83–93.
- [15] Xie, X.-F., S. F. Smith, and G. J. Barlow, Schedule-Driven Coordination for Real-Time Traffic Network Control. In *ICAPS*, 2012.
- [16] Smith, S., G. Barlow, X.-F. Xie, and Z. Rubinstein, SURTRAC: Scalable Urban Traffic Control. In *Transportation Research Board 92nd Annual Meeting Compendium of Papers*, Transportation Research Board, 2013.
- [17] Daganzo, C. F., The cell transmission model: A dynamic representation of highway traffic consistent with the hydrodynamic theory. *Transportation Research Part B: Methodological*, Vol. 28, No. 4, 1994, pp. 269–287.
- [18] Daganzo, C. F., The cell transmission model, part II: network traffic. *Transportation Research Part B: Methodological*, Vol. 29, No. 2, 1995, pp. 79–93.

- [19] Xiaojian, H., W. Wei, and H. Sheng, Urban traffic flow prediction with variable cell transmission model. *Journal of Transportation Systems Engineering and Information Technology*, Vol. 10, No. 4, 2010, pp. 73–78.
- [20] Sumalee, A., R. Zhong, T. Pan, and W. Szeto, Stochastic cell transmission model (SCTM): A stochastic dynamic traffic model for traffic state surveillance and assignment. *Transportation Research Part B: Methodological*, Vol. 45, No. 3, 2011, pp. 507–533.
- [21] Jabari, S. E. and H. X. Liu, A stochastic model of traffic flow: Theoretical foundations. *Transportation Research Part B: Methodological*, Vol. 46, No. 1, 2012, pp. 156–174.
- [22] Huang, K. C., *Traffic Simulation Model for Urban Networks: CTM-URBAN*. Ph.D. thesis, Concordia University, 2011.
- [23] Muralidharan, A., G. Dervisoglu, and R. Horowitz, Freeway traffic flow simulation using the link node cell transmission model. In *American Control Conference, 2009. ACC'09.*, IEEE, 2009, pp. 2916–2921.
- [24] Gomes, G. and R. Horowitz, Optimal freeway ramp metering using the asymmetric cell transmission model. *Transportation Research Part C: Emerging Technologies*, Vol. 14, No. 4, 2006, pp. 244–262.
- [25] Kim, Y., *Online traffic flow model applying dynamic flow-density relation*. Int. At. Energy Agency, 2002.
- [26] Lu, S., S. Dai, and X. Liu, A discrete traffic kinetic model—integrating the lagged cell transmission and continuous traffic kinetic models. *Transportation Research Part C: Emerging Technologies*, Vol. 19, No. 2, 2011, pp. 196–205.
- [27] Alecsandru, C., A. Quddus, K. C. Huang, B. Rouhieh, A. R. Khan, and Q. Zeng, An assessment of the cell-transmission traffic flow paradigm: Development and applications. In *Transportation Research Board 90th Annual Meeting*, 2011, 11-1152.